Full Paper

Propellants, Explosives, Pyrotechnics

DOI: 10.1002/prep.201300176

Fabrication, Thermoanalysis, and Performance Evaluation Studies on RDX-based Microcellular Combustible Objects

Weitao Yang,[a] Yuxiang Li,[a] and Sanjiu Ying*[a]

Abstract: In the development of weapons, the current trend is to replace incombustible constituent elements with combustible ones. The traditional porous combustible objects are composed of nitrocellulose as energetic component, which is highly sensitive and inflammable. Formulations composed of high content RDX and inert polymer binder were employed to replace the tradional ones. This paper reports the fabrication process of microcellular combustible objects with skin-core structure using supercritical CO_2 (SC-CO_2) as foaming agent. The objects were foamed in designed foaming molds with expansion ratios of 1.1, 1.2 and 1.35. The influence of foaming temperature, saturation pressure, expansion ratio and RDX content on porous structure was investigated by scanning electron microscopy (SEM). Thermogravimetric analysis was conducted and the results revealed a two-stage decomposition process of RDX and binder. Performance in terms of heat resistance and moisture resistance was evaluated and compared with the traditional ones. A comparative study indicated that microcellular combustible objects are superior to traditional ones in respect of their survivability.

Keywords: Microcellular combustible objects · Manufacturing process · Supercritical CO_2 · Thermogravimetric analysis · Performance evaluation

1 Introduction

In the development of weapons, the replacement of constituent elements of ammunition which, until recently, were made of an incombustible metal or non-metal, by combustible elements which decompose by burning when the ammunition is fired has become increasingly common. Combustible cartridges are mainly used as combustible objects in weaponry, additionally, caseless ammunition and combustible detonator-holding tubes are known.

In the past, felted, combustible cases were fabricated from a mixture of nitrocellulose fibers and cellulose fibers, which were investigated in prior studies [1–3]. However, the ammunition is easily ignited due to the highly sensitive and inflammable property of the nitrocellulose component when left in contact with the hot mechanical part in weaponry. In addition, due to the presence of the hygroscopic cellulosic fibrous material, such cases on exposure to moisture readily absorb water with consequent loss of strength, dimensional stability and combustibility, which can lead to disastrous accidents. Hence, the application of a formulation resembling a low-vulnerability propellant [4–6] with low vulnerability, high ignition temperature and good heat/moisture resistance can solve the above problems.

It is evident that an appropriate density is a critical requirement for the objects to eliminate smoke and obtain complete consumption of the objects in the weapons. In recent years, researchers have produced foamed thermoset PU bonded RDX caseless ammunition by reaction injection molding (RIM) process [7,8]. A physical method to fabricate microcellular combustible objects using supercritical CO_2 (SC-CO_2) as foaming agent presents an obvious environmental advantage over conventional chemical foaming agents. Supercritical CO_2 exists as a non-condensable, high-density fluid above the critical temperature (31.1 °C) and critical pressure (7.4 MPa) and offers many desirable properties as both solvents and foaming agents including adjustable solvent strength [9–11], efficient plasticization [12–14], and enhanced diffusion rates [10,15]. A microcellular object usually contains more than 10^9 microcells per cm^3 [16], which provide higher impact strength [17] and act as a heat insulator. Since CO_2 is a gas at ambient conditions, the solvent rapidly dissipates upon release of pressure. A pressure quench from supercritical conditions at constant temperature also ensures that no vapor/liquid boundary is encountered which can damage the cellular structure of a pore. Moreover owing to the thermoplastic polymer binder, the non-ideal combustible objects can be made into dough again by solvent and extruded into new products instead of centralized burning treatment.

Generally, the foamed objects should be processed into a desired shape before being applied in weaponry. The

[a] *W. T. Yang, Y. K. Li, S. S. Ying*
School of Chemical Engineering
Nanjing University of Science and Tehnology
Nanjing. 210094. P. R. China
**e-mail: yingsanjiu@126.com*

 © 2014 Wiley-VCH Verlag GmbH & Co. KGaA, Weinheim

foamed objects can be lathed into the required shape from bulks, which is hazardous for machinists. In this study, the objects were foamed in designed foaming molds to fabricate microcellular combustible objects with required shapes. Hence, the objective of the paper is to study the feasibility of the novel fabrication process and to study the influence of molds restraint and foaming conditions on porous structures. Thermogravimetric analysis and performance evaluation studies of the objects we are also conducted.

2 Experimental Section

2.1 Preparation of Samples

2.1.1 Density Control

In the free foaming process, the sample was foamed without restraint, and the cells grew completely. Nevertheless, in the confined foaming process, with the restriction of the walls of the molds, the sample with thickness h_0 was foamed in the space between outer plate and inner plate with distance h, as shown in Figure 1. Expansion ratio refers to the ratio of the volume of the foamed sample relative to that of the un-foamed one with the same mass, i.e. the ratio of h to h_0. In this study, three molds with expansion ratio of 1.1, 1.2 and 1.35 were adopted to fabricate microcellular combustible objects with different densities, which are shown in Table 1.

2.1.2 Solvent and Extruding Process

Three compositions based on RDX of average grain diameter of 10 μm, inert thermoplastic polymer and additives were formulated with a varying percentage of RDX. The formulations were prepared into dough by a solvent process using acetone as solvent, and then, the dough was extruded into the preform with desired shape with thickness of 2.0 mm. The preform was dried until the volatile content less than 0.5 %.

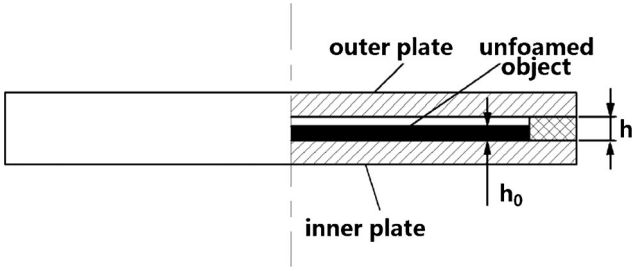

Figure 1. Schematic diagram of the foaming mold.

Table 1. Sample densities [g cm^{-3}].

RDX ratio	Unfoamed	Expansion ratio		
		1.1	1.2	1.35
50 %	1.36	1.24	1.13	1.01
60 %	1.49	1.35	1.24	1.10
70 %	1.61	1.46	1.34	1.19

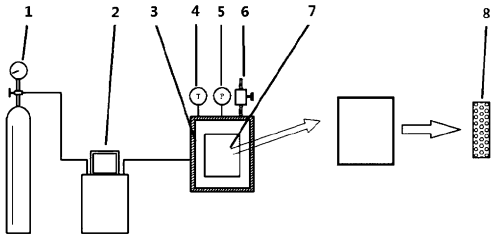

1. CO_2 cylinder 2. plunger type metering pump 3. high pressure vessel 4. thermometer 5. pressure gauge 6. vent 7. foaming mould 8. foamed sample

Figure 2. Schematic illustration of the foaming process in SC-CO2.

2.1.3 Rapid Decompression Foaming Process

Figure 2 presents the schematic illustration of the foaming process. Firstly, the high pressure vessel was preheated to a desired temperature above critical temperature. Subsequently, the preform was placed into the foaming mold. After being flushed for a few minutes with CO_2, the vessel was pressurized to the desired pressure by supercritical fluid equipment. The foaming mold containing the preform was exposed in SC-CO_2 for a prescribed saturation time (10 h). Finally, the vent of the vessel was opened and the pressure was quenched rapidly to atmospheric conditions within 30 seconds. The foaming mold was placed at atmospheric pressure for 0.5 h so that most of the residual gases would seep from the cells and matrix and the cells were frozen.

2.2 Porous Characterization

The samples were freeze-fractured in liquid nitrogen and sputter-coated with gold. The surface of the sample was sputter-coated with gold directly. The inner and surface morphology of sample was observed with a QUANTA FEG 250 scanning electron microscope (SEM).

2.3 Thermal Studies

Thermal decomposition of the samples was studied thermogravimetrically at a heating rate of 10 K min^{-1}, using a thermal analysis system of TA Q600 DSC/TGA in nitrogen atmosphere (sample mass 2–3 mg).

2.4 Hot Plate Test

The samples were tested on a heating plate at various temperatures to study the heat resisting property compared

 © 2014 Wiley-VCH Verlag GmbH & Co. KGaA, Weinheim

with felted one. The test pieces were placed, at normal pressure, in contact with the heating plate at the temperature of the experiment, the surface being placed against the metal. The self-ignition delay of each test piece was measured.

2.5 Moisture Absorption Test

The hygroscopic properties of the samples were studied by the weight method. The samples were placed in a weighting bottle, and dried at 55 °C for 48 h. Afterwards, the samples we are transferred to the thermostatic and humidistatic chamber. The temperature was 30 °C and the relative humidity (RH) was (90.0 ± 3.0)%. The moisture absorption rate was calculated by Equation (1).

$$Q_x = (\omega_2 - \omega_1)/\omega_1 \times 100\,\% \quad (1)$$

Where Q_x is the moisture absorption rate, ω_1 is the weight of the dried sample, ω_2 is the weight of the humid sample.

3 Results and Discussion

3.1 Unfoamed Sample

Dispersion of RDX particles in polymer matrix before foaming was characterized firstly because of its importance in the properties of microcellular samples. Figure 3 shows the micrograph of unfoamed sample with RDX ratio of 60% after the solvent and extruding process. It reveals that RDX particles are uniformly and discretely dispersed in the matrix without agglomeration.

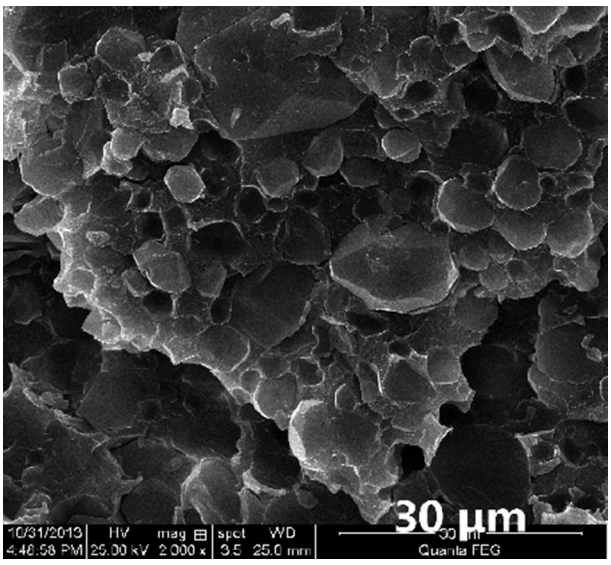

Figure 3. SEM micrograph of the unfoamed sample.

3.2 Influence of Foaming Temperature

Generation of cells on the surface of RDX particles and in the polymer matrix, i.e. heterogeneous and homogeneous nucleation do as not occur simultaneously, because the energy-barrier for heterogeneous nucleation is three orders of magnitude lower than that of homogeneous one [18]. Therefore, the preferential heterogeneous nucleation of cells and subsequent cell growth consumes a large amount of gas contiinly, resulting in deficiency of gas in polymer matrix. Hence, homogeneous nucleation will not generate until the nucleation rate is high enough, which is mainly influenced by the foaming temperature [19,20]. Increasing the temperature also decreases the viscosity of the binder, causing the retractive force restricting cell growth to decrease and the diffusivity of CO_2 within the matrix to increase. In addition, the higher the temperature, the longer the time (at a given decompression rate) cells have to grow before vitrification.

Figure 4 shows micrographs of foamed samples foamed from 40 to 70 °C with a magnification of ×2000. As depicted in Figure 4, when the foaming temperature was 40 °C, only heterogeneous nucleation around RDX particles occurred, and the cell wall was solid without cells. When the temperature increased, the samples presented a clear bimodal cell structure composing of cells generated by heterogeneous and homogeneous nucleation. Besides, the experimental results in Figure 4 also show that the cell size generated by both heterogeneous and homogeneous nucleation increases with foaming temperature. With increasing cell size, the cells would collapse and combine, resulting from the fixed expansion ratio.

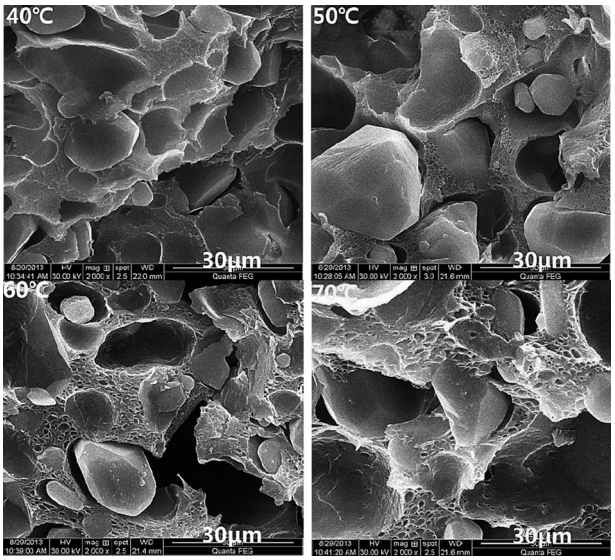

Figure 4. SEM micrographs of foamed samples with different foaming temperatures (RDX ratio = 60%, saturation pressure = 15 MPa, expansion ratio = 1.35).

 © 2014 Wiley-VCH Verlag GmbH & Co. KGaA, Weinheim

3.3 Influence of Saturation Pressure

An increasing saturation pressure causes an increase in the sorption amount of CO_2, which affects the plasticization of polymer binder [12–14]. The plasticization is weakened with the diffusion of gas into the cells during the cell growth. The cells stop growing due to vitrification of polymer.

Figure 5 shows the micrographs of samples foamed at 40 °C after being saturated at different pressure. Cells of foamed samples saturated under 5 MPa are smaller than those of samples saturated at supercritical fluid condition. In addition, the preform saturated under 5 MPa failed to expand to the desired thickness in the mold after foaming. The experiment results show that the saturation pressure has limited influence on the plasticization after 10 MPa, which is in agreement of the results reported by Ruiz [21] and Goel [12].

3.4 Samples with Various Expansion Ratios

The molds with certain expansion ratio determine the foaming space of the saturated preform. The cells grow with the restriction of mold walls. Increasing the expansion ratio means increasing the porosity and decreasing the relative density.

Figure 6 and Figure 7 show the influence of expansion ratio on sample porous structure. As indicated in Figure 6, the cells size and the interval of between RDX particle and polymer matrix decreased with decreasing expansion rate and the objects appeared more compact. As shown in Figure 7, the samples foamed at 60 °C have a bimodal cellular structure. The density of homogeneous cells of sample

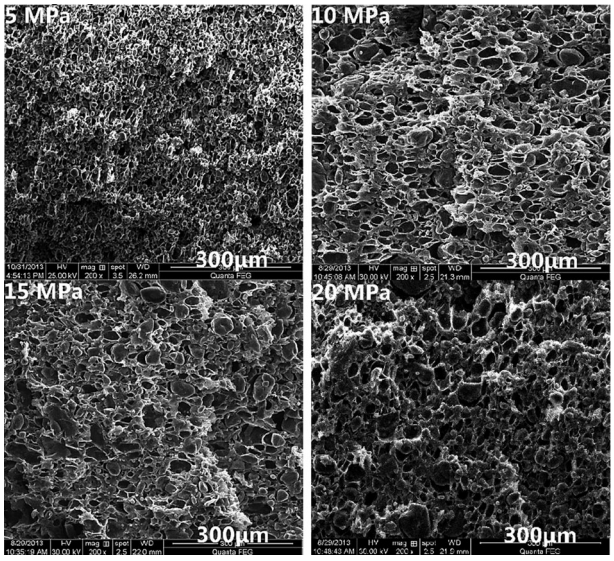

Figure 5. SEM micrographs of foamed samples with saturation pressure (RDX ratio = 60 %, expansion ratio = 1.35, foaming temperature = 40 °C).

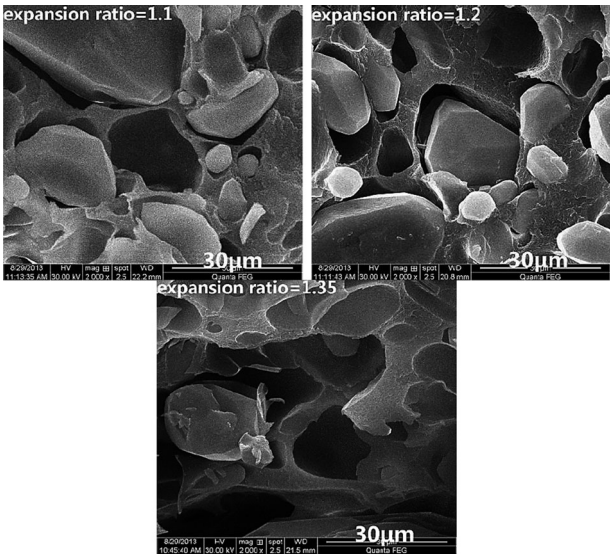

Figure 6. SEM micrographs of foamed samples with different expansion ratios foamed at 40 °C (RDX ratio = 60 %, saturation pressure = 15 MPa).

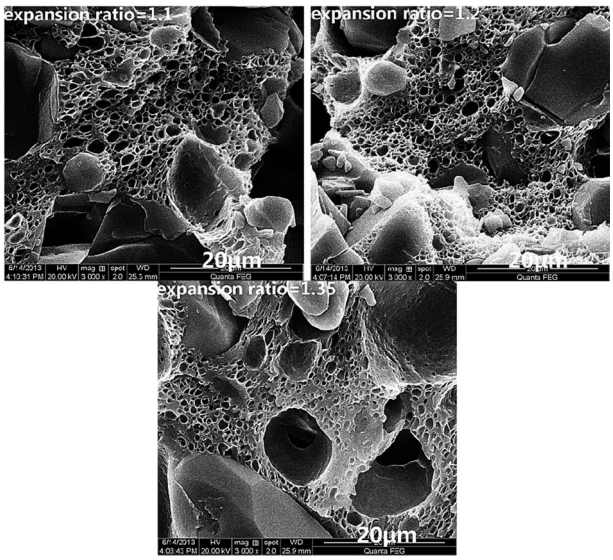

Figure 7. SEM micrographs of foamed samples with different expansion ratios foamed at 60 °C (RDX ratio = 60 %, saturation pressure = 15 MPa).

with expansion ratio of 1.35 seems lower than that of samples with lower expansion ratio. Compared with samples foamed at 40 °C in Figure 6, the influence of expansion ratio became not obvious and the space between RDX and polymer seems smaller due to the increased viscosity at higher foaming temperature.

3.5 Influence of RDX Contents

More RDX particles in sampels provide more sites for cells to nucleate and grow, resulting in more cells in per unit

 © 2014 Wiley-VCH Verlag GmbH & Co. KGaA, Weinheim

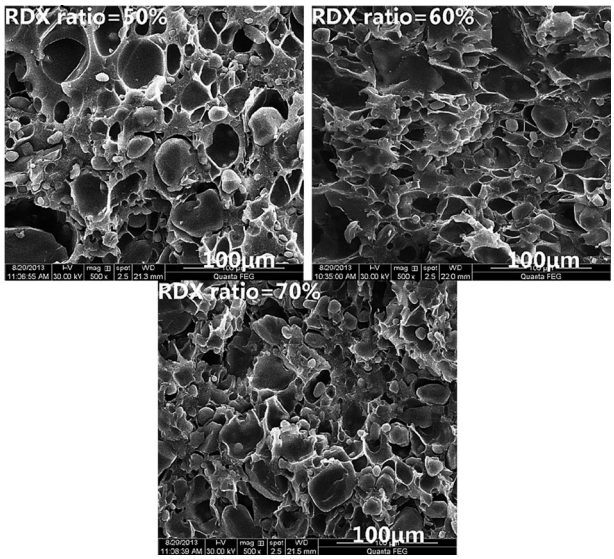

Figure 8. SEM micrographs of foamed samples with various RDX content (expansion ratio = 1.35, foaming temperature = 40 °C, saturation pressure = 15 MPa).

volume under the same expansion ratio. Figure 8 shows the SEM micrographs of microcellular samples as a function of RDX ratio. As Figure 8 reveals, with the increasement of RDX content, the cell density increased and the cell size decreased.

3.6 Skin-core Structure

Figure 9 shows SEM micrographs of skin-core structure of these objects. In the pressure quench process, the gas expansion absorbed heat and led to the decrease of temperature in vessel [21], which is much lower than the effective glass-transition temperature. Consequently, an unfoamed skin with thickness of about 100 μm was generated.

3.7 Thermogravimetric Analysis

Figure 10 shows the TG curves of samples with RDX contents of 50, 60, and 70%, compared with pure RDX and the binder. The decomposition procedure was composed of decomposition of RDX with a wide temperature range of 196 to 250 °C and the decomposition of binder from 270 to about 420 °C. In addition, compared with the curve of pure RDX, the decomposition of the samples was delayed, which may be influenced by the nearby binder around the RDX particles.

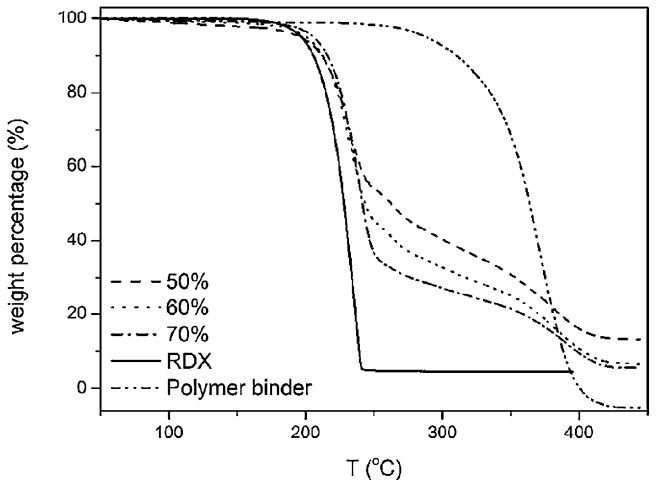

Figure 10. TG curves of the samples and raw materials.

3.8 Hot Wall Tests

Heat resistance was an important property to safe use when the object contact with hot mechanical part, such as hot gun chamber of high-rate-fire gun when the objects were used as caseless ammunition or combustible cartridge case.

Table 2 shows the values of ignition delay time when the objects were contact with hot wall with various temperatures. As shown in the Table the ignition delay time increase obviously compare with felted case, resulting from the skin protection and the heat resistance property of the formulation. When the temperature is 200 °C, the objects were not ignited in 3 min, except for expansion. The delay time is enough for the feeding of the ammunition without menace of preignition.

3.9 Moisture Absorption

Figure 11 shows the moisture absorption of felted case and microcellular objects which were foamed at 60 °C with ex-

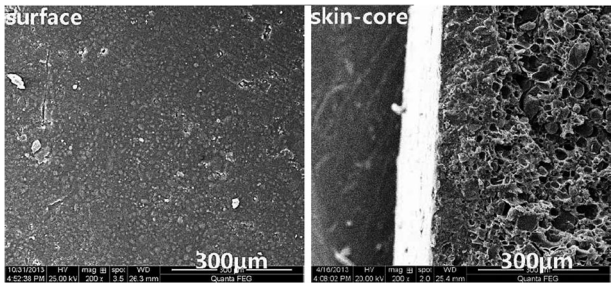

Figure 9. SEM micrographs of the skin-core structure.

Table 2. Values of ignition delay time.

Samples	Temperature			
	200 °C	250 °C	300 °C	350 °C
Felted case	43.9 s	20.1 s	4.6 s	1.7 s
50%		50.9 s	15.6 s	8.9 s
60%	Not ignited in 3 min	48.2 s	10.7 s	8.0 s
70%		47.5 s	9.8 s	7.9 s

 © 2014 Wiley-VCH Verlag GmbH & Co. KGaA, Weinheim

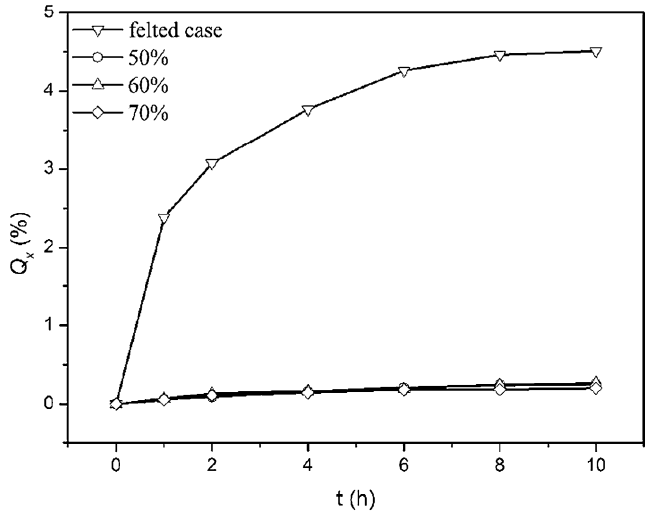

Figure 11. Hygroscopicity curves of the microcellular and felted samples.

pansion ratio 1.2. The microcellular objects has a low moisture absorption rate less than 0.5 % with the protection of skin, which eliminate moisture absorption and form a completely water proof cover. Nevertheless, the felted one absorbed moisture quickly and absorbed 10 times more moisture than the former one.

4 Conclusion

RDX-based microcellular combustible objects were fabricated by a novel preparation method using SC-CO_2 as foaming agent. The objects have unfoamed skin and contain a number of isolated microcells. The porous structure can be controlled by expansion ratio as well as foaming condition to meet different requirements. Experimental results revealed that the objects have a high decomposition temperature and good heat/moisture resistant property. This method can be applied to fabricate combustible constituent elements to replacing the traditional one.

Acknowledgments

Funding by the Priority Academic Program Development of Jiangsu Higher Education Institutions is gratefully acknowledged.

References

[1] G. R. Kurulkar, R. K. Syal, H. Singh, Combustible Cartridge Case Formulation and Evaluation, *J. Energ. Mater.* **1996**, *14*, 127–149.

[2] P. L. Deluca, J. C. Williams, Fibrillated Polyacrylic Fiber in Combustible Cartridge Cases, *Ind. Eng. Chem. Prod. Res. Dev.* **1984**, *23*, 438–441.

[3] M. S. Nusbaum, Theoretical Analysis of a Fully Combustible Telescoped Round, *J. Spacecr. Rockets* **1969**, *6*, 84–86.

[4] A. G. S. Pillai, R. R. Sanghavi, C. R. Dayanandan, M. M. Joshi, S. P. Velapure, A. Singh, Studies on RDX Particle Size in LOVA Gun Propellant Formulations, *Propellants Explos. Pyrotech.* **2001**, *26*, 226–228.

[5] R. R. Sanghavi, P. J. Kamale, M. A. R. Shaikh, S. D. Shelar, K. S. Kumar, A. Singh, HMX Based Enhanced Energy LOVA Gun Propellant, *J. Hazard. Mater.* **2007**, *143*, 532–534.

[6] R. S. Damse, A. Singh, H. Singh, High Energy Propellants for Advanced Gun Ammunition Based on RDX, GAP and TAGN Compositions, *Propellants Explos. Pyrotech.* **2007**, *32*, 52–60.

[7] J. Böhnlein-Mauß, A. Eberhardt, T. S. Fischer, Foamed Propellants, *Propellants Explos. Pyrotech.* **2002**, *27*, 156–160.

[8] J. Böhnlein-Mauß, H. Kröber, Technology of Foamed Propellants, *Propellants Explos. Pyrotech.* **2009**, *34*, 239–244.

[9] R. G. Wissinger, M. E. Paulaitis, Swelling and Sorption in Polymer–CO_2 Mixtures at Elevated Pressures, *J. Polym. Sci., Part B: Polym. Phys.* **1987**, *25*, 2497–2510.

[10] A. R. Berens, G. S. Huvard, R. W. Korsmeyer, F. W. Kunig, Application of Compressed Carbon Dioxide in the Incorporation of Additives into Polymers, *J. Appl. Polym. Sci.* **1992**, *46*, 231–242.

[11] S. R. Allada, Solubility Parameters of Supercritical Fluids, *Ind. Eng. Chem. Process Des. Dev.* **1984**, *23*, 344–348.

[12] S. K. Goel, E. J. Beckman, Plasticization of Poly(methyl Methacrylate) (PMMA) Networks by Supercritical Carbon Dioxide, *Polymers* **1993**, *34*, 1410–1417.

[13] P. Alessi, A. Cortesi, I. Kikic, F. Vecchione, Plasticization of Polymers with Supercritical Carbon Dioxide: Experimental Determination of Glass-transition Temperatures, *J. Appl. Polym. Sci.* **2003**, *88*, 2189–2193.

[14] M. A. Fanovich, P. Jaeger, Sorption and Diffusion of Compressed Carbon Dioxide in Polycaprolactone for the Development of Porous Scaffolds, *Mater. Sci. Eng. C* **2012**, *32*, 961–968.

[15] M. Tang, T.-B. Du, Y.-P. Chen, Sorption and Diffusion of Supercritical Carbon Dioxide in Polycarbonate, *J. Supercrit. Fluids* **2004**, *28*, 207–218.

[16] S. Ito, K. Matsunaga, M. Tajima, Y. Yoshida, Generation of Microcellular Polyurethane with Supercritical Carbon Dioxide, *J. Appl. Polym. Sci.* **2007**, *106*, 3581–3586.

[17] L. M. Matuana, Solid State Microcellular Foamed Poly(lactic Acid): Morphology and Property Characterization, *Biores. Technol.* **2008**, *99*, 3643–3650.

[18] J. S. Colton, N. P. Suh, Nucleation of Microcellular Foam: Theory and Practice, *Polym. Eng. Sci.* **1987**, *27*, 500–503.

[19] S. K. Goel, E. J. Beckman, Generation of Microcellular Polymeric Foams using Supercritical Carbon Dioxide. I: Effect of Pressure and Temperature on Nucleation, *Polym. Eng. Sci.* **1994**, *34*, 1137–1147.

[20] J. S. Colton, N. P. Suh, The Nucleation of Icrocellular Thermoplastic Foam: Process Model and Experimental Results, *Adv. Manuf. Process.* **1986**, *1*, 341–364.

[21] J. A. R. Ruiz, M. Pedros, J. M. Tallon, M. Dumon, Micro and Nano Cellular Amorphous Polymers (PMMA, PS) in Supercritical CO_2 Assisted by Nanostructured CO_2-philic Block Copolymers-One Step Foaming Process, *J. Supercrit. Fluids* **2011**, *58*, 168–176.

Received: November 18, 2013
Revised: December 9, 2013
Published online: January 20, 2014

 © 2014 Wiley-VCH Verlag GmbH & Co. KGaA, Weinheim